



Experimental study of droplet temperature in a two-phase heptane/air V-flame



Camille Letty, Bruno Renou^{*}, Julien Reveillon, Sawitree Saengkaew, Gérard Gréhan

CORIA UMR 6614, CNRS, INSA de Rouen, 76801 Saint Etienne du Rouvray, France

ARTICLE INFO

Article history:

Received 30 May 2011

Received in revised form 23 August 2012

Accepted 14 March 2013

Available online 9 May 2013

Keywords:

Two-phase combustion

Global rainbow technique

Droplet temperature

ABSTRACT

An understanding of the complex phenomena involved in droplet combustion, such as two-phase flows and heat/mass transfer, is a necessary step towards improving combustion efficiency and reducing pollutant emissions. This paper is focused on an analysis of the droplet temperature evolution across the flame front in two-phase flow systems. In this experiment, the flame was stabilized on a rod at atmospheric pressure and the fuel was liquid at injection, which implies the presence of fuel droplets close to the flame front. However the flame was partially premixed because part of the fuel vaporized quickly and contributed to the stabilization of the flame. The configuration was two-dimensional and so called “V-shape” flame. Two different flow conditions were investigated: a pseudo-laminar flow as the reference case (R) and a low-turbulence level flow (LT). The evolution of the mean fuel droplet temperature across the flame brush was quantified. The shape of the fuel droplet temperatures histogram became clearly bimodal for high values of the mean progress variable \bar{c} , indicating the presence of droplets in the measurement volume that were heated up by the burnt gases and the flame. The temperature evolution and the statistics across the flame front can be used to compare the numerical and the physical models applied to two-phase combustion.

© 2013 The Combustion Institute. Published by Elsevier Inc. All rights reserved.

1. Introduction

Turbulent spray combustion is used extensively to convert energy in such practical applications as furnaces, gas turbines, and aeronautic or automotive engines. Nowadays these installations have to meet very strict economical and environmental specifications. To comply with these restrictions requires an in-depth understanding and modeling of the various physical phenomena interacting in the combustion chamber, which is fed by a liquid fuel. Two-phase combustion is a complex phenomenon involving the dispersion and the evaporation of a liquid fuel in a gaseous oxidizer. Capturing the mass and heat exchange between both phases is of primary importance to predict the topology of the gaseous fuel and the resulting combustion regimes. Nevertheless, a substantial lack of information regarding the various exchanges between the liquid and the gas phase, and their direct impact on the combustion processes, persists as a result of experimental and modeling difficulties, which arise from the simultaneous presence of the two phases. Although numerical simulation is a valuable tool to overcome many of these measurement difficulties, the method still

needs to be validated through sound experimental studies. Furthermore, it is not yet able to tackle very complex configurations. It is therefore of fundamental interest to develop experimental set-up that are able to capture and analyze the various interactions between the liquid and gas phases in spray combustion.

Previous studies dedicated to two-phase combustion have considered generic configurations such as dilute laminar spray diffusion flames in a coflow configuration [1] or counter-flow diffusion spray flames [2]. Various combustion regimes have also been studied (for instance, partially pre-vaporized sprays [3], partially premixed spray jets [4], and swirling flames [5,6] leading to partially premixed combustion). These experiments, dedicated to several aspects of two-phase combustion, were focused on five main areas of study: (i) the combustion regimes and the transitions between them, (ii) the flame structures that resulted from the droplet diameter and the presence of droplets close to the flame front, (iii) the relationships between strain rate and burning velocity or temperature, (iv) the evolution of droplet velocity and size distribution during the combustion process, (v) the ignition of flame kernels.

One of the fundamental aspects to consider in two-phase flow combustion is the heat transfer between the liquid and the gas phase that necessarily occurs during the vaporization process. Generally the temperature of the liquid phase injected into the combustion chamber is below the gas phase temperature. Most

^{*} Corresponding author. Address: CNRS UMR 6614, CORIA, Université et INSA de Rouen, Site Universitaire du Madrillet, BP 12, 76801 Saint-Etienne du Rouvray Cedex, France. Fax: +33 2 32 96 97 80.

E-mail address: bruno.renou@coria.fr (B. Renou).

importantly its concentration in the gas phase is below its liquid saturation level. As a result the temperature difference between liquid and gas induces heat transfer immediately. Part of the energy reaching the droplets participates in the vaporization process proportionally to the latent heat of vaporization, whilst the remaining part increases the liquid temperature within the limits of the saturation level. This energy, which is necessary for the liquid vaporization, is provided by the gas phase surrounding the droplets or clusters of droplets. Therefore a local decrease of the temperature level follows; it may have a substantial effect on the combustion process. This phenomenon forms the basis of the flame extinction process through water sprays and is the subject of a wide range of works in this field (see [7] and reference therein). The engine community is mainly concerned with the absorption of energy by fuel droplets, which may lead to considerable variations in the combustion process. This occurrence can be analyzed through two stages: the ignition process and the flame propagation.

Literature about numerical [8,9] and experimental [10,11] work on two-phase flow autoignition is still scarce, and only a few general trends are known. The influence of temperature, pressure, and droplet size was discussed by Aggarwal [12]. A recent study [13] specifically concerned with the temperature effect has shown a strong level of interaction between three main phenomena (based on three characteristic delays): the vaporization process (τ_v), the first increase of the mixture temperature of about 200 K (cool flame, τ_{cf}), and the final chemical runaway (autoignition, τ_{ai}). If the three corresponding characteristic delays are well-segregated ($\tau_v < \tau_{cf} < \tau_{ai}$), it is possible to observe a correspondence between the gaseous and the two-phase flow autoignition delays through the introduction of a temperature shift due to the preliminary cooling effect. On the contrary, if all of these characteristic delays are of the same order of magnitude, significant interactions occur that make the prediction of the two-phase flow results (based on the gaseous phase) much more difficult even if heat transfer is well known. Indeed, the phenomena are highly non-linear because a variation in mixture temperature of a few degrees can significantly modify the autoignition delay. Thus it emphasizes the importance of a proper estimation of heat transfer between the liquid and the gas phases.

In addition to autoignition, flame propagation is also strongly affected by the heat transfer processes: on one hand, it modifies the temperature of the mixture and on the other hand it also affects the mixture itself, which characteristics depend on the liquid vaporization rate. Therefore, local flame extinction or acceleration may occur along with modifications of the flame structure and the combustion regime, as was shown in [14]. Prior to this work, Chiu et al. [15] first, then, Chang and Borghi [16,17], determined the structure of flames propagating through a cloud of droplets injected into a preheated oxidizer. Because of the heat transfer processes between the cloud and the oxidizer two main combustion regimes were detected according to the droplet mean inter-space: (i) group combustion occurs when the droplets are too close to each other to allow heat diffusion inside the cloud. Hence only an external layer of droplets is vaporized and the flame remains at a standoff distance from the spray boundary, (ii) individual droplet burning happens when the droplets are sparse enough and hot gases are able to reach the core of the spray. Vaporization and combustion processes therefore take place around every individual droplet.

The analytical and numerical works mentioned above lack of experimental data that are necessary to validate and extrapolate the results to more complex configurations. More specific information on both liquid and gas phase temperatures is necessary to characterize heat transfer. This is also required to develop and validate appropriate vaporization, ignition, and combustion models that take the thermodynamical processes at the liquid interface

into account. Thus the objective of this paper is to propose a first step in this direction by presenting an experimental set-up based on rainbow refractometry to measure the evolution of the liquid temperature in a complete spray and in a V-shape flame configuration that can be easily used for numerical simulations. Different research teams have developed various techniques to extract the temperature of spray droplets, including infrared emission [18], morphology dependent resonance [19,20], Raman scattering [21], two-color laser induced fluorescence [22] and global rainbow refractometry [23,24]. The global rainbow technique (GRT) was introduced by Van Beeck et al. [25] and appears to be very promising. In this paper, the experimental set-up designed for two-phase combustion and the optical diagnostics used to fully characterize the flame are presented.

First, the experimental set-up is described with an emphasis on the global rainbow technique used to determine the temperature distribution in the spray of droplets. Then detailed results are presented and analyzed from the basic properties of the flow to the spray temperature distribution. Two turbulence levels and two heights above the anchorage point of the V-shape flame are described here.

2. Experimental methods

2.1. Experimental setup

Experiments were carried out in a vertical wind-tunnel with a square section ($8 \times 8 \text{ cm}^2$) designed for the study of steady combustion [26,27]. Air was regulated via a Bronkhorst mass flow controller (F-206A1). The flow was directed to a divergent/convergent chamber. A bed of glass beads and honeycombs were used to attenuate residual turbulent perturbations. The flow was then accelerated through a convergent (aspect ratio contraction 11:1). In the absence of any obstacle, the residual turbulence level was as low as 0.4%. The liquid fuel (N-heptane) was stored in a pressurized tank (up to 6 bar). An electronic mass flow controller (Bronkhorst, LIQUI-FLOW L30, [0.0–6.0] kg/h) regulated the liquid flow. A fuel atomizer (Delavan, 3.78 L/h, hollow cone, 80° angle) was centered in the chamber 600 mm under the exit of the wind tunnel and was used to generate n-heptane droplets. Droplets spread outside the burner within one third of the burner exit section width (Fig. 1a). A 2D stationary V-shape flame was stabilized on a thin rod (2 mm in diameter) placed in the middle plane of the exit section. Figure 1b specifies the direction of the axis and the notations used in this paper.

Two different flow conditions were investigated in this study. The air flow rate was constant and set to $87.3 \text{ m}^3/\text{h}$. At the exit of the convergent, the air flow temperature without fuel droplets was measured prior to each experiment at $19 \pm 1 \text{ }^\circ\text{C}$. The mass flow rate of liquid N-heptane was fixed for both conditions and equal to 1.4 kg/h . The reference case was a pseudo-laminar flow (hereinafter R); it corresponds to the case for which no grid is placed at the exit of the burner. The second case was a low-turbulence condition (hereinafter LT). A grid was used to generate turbulence and was placed between the outlet of the convergent and the rod. This grid consists of 3-mm diameter rods distributed on two levels, with a solidity of 51% and a mesh size of 10 mm. Measurements are presented in a Cartesian coordinate system (except if specified otherwise); the origin of the Cartesian coordinate system is the rod.

2.2. Optical diagnostics

The size distribution of the fuel droplets was determined with a diffraction method (Malvern Spraytec 97, EPCS-F model). The laser was characterized by a 10 mm in-diameter low power beam and a

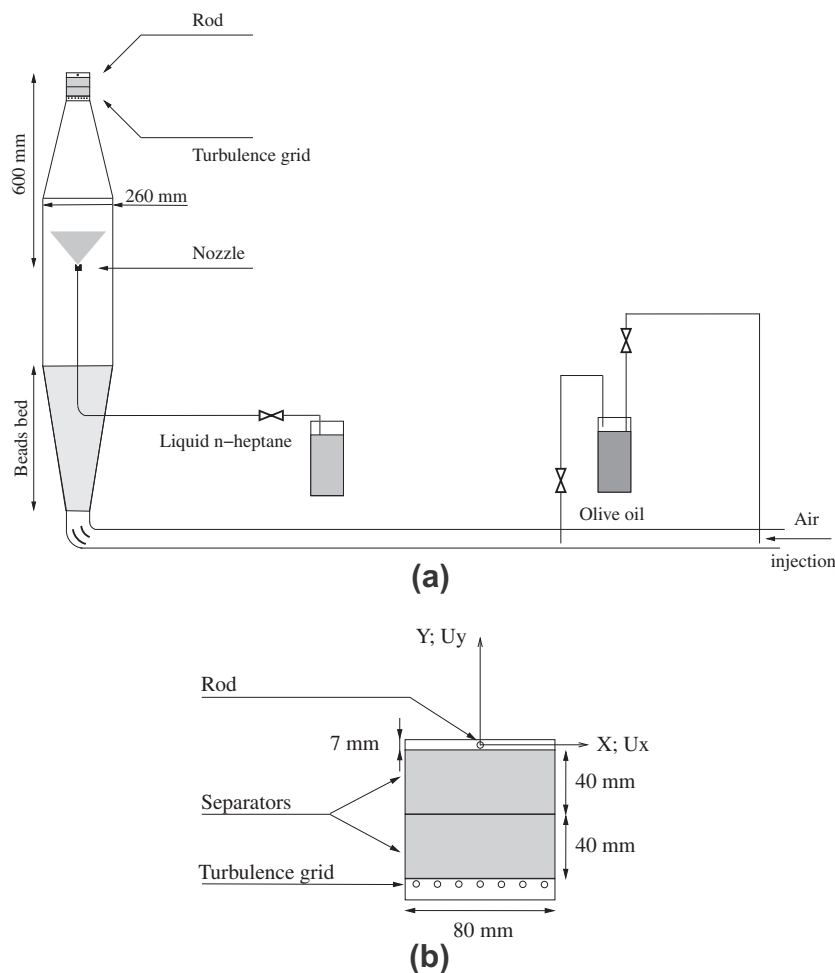


Fig. 1. Experimental setup. (a) Sketch of the burner for the stabilization of two-phase flames with the air deviation to the seeding (olive oil for PIV). (b) Detail of the exit section of the burner.

wavelength of $\lambda = 670 \mu\text{m}$. The Malvern instrument enabled us to detect droplets in a wide range of diameters. In this study, the focal length of the device ($f = 200 \text{ mm}$) corresponded to diameters ranging from 5 to $500 \mu\text{m}$. Acquisitions were recorded at 100 Hz and each measure was integrated both in time and space. Measurements were performed in two horizontal planes parallel to the exit section of the burner (at $y = 35 \text{ mm}$ and at $y = 55 \text{ mm}$; Fig. 4, red dots). Three different locations were scrutinized at each level: centered in the exit section ($x = 0 \text{ mm}$), 10-mm shifted ($x = 10 \text{ mm}$), and 15-mm shifted ($x = 15 \text{ mm}$).

The spatial velocity field in the non-reactive configuration was investigated via particle image velocimetry (PIV) with an Nd-Yag laser (Big Sky laser, 120 mJ/pulse, 532 nm) used as a light source. The vertical laser sheet coincided with the middle plane of the exit of the burner. Light scattered by olive oil droplets was recorded with a CCD camera (FlowMaster LaVision, 12 bits, 1280×1024 pixels) equipped with a 50 mm $f/1.2$ Nikkor lens. The magnification ratio was 25 pix/mm. Particle images were post-processed with the standard commercial package available in Davis 6.2 (LaVision Company). Velocity field computations were based on a multi-pass algorithm with adaptive window deformation [28]. The starting and final interrogation windows were set to 64×64 pix and 32×32 pix respectively, with a 50% overlap.

Although the flame was stabilized in a two-phase flow, it can be considered as a partially premixed flame because part of the liquid fuel vaporized quickly and mixed with air before reaching the rod (stabilization zone). Premixed flames are usually described

through the Reynolds averaged progress variable \bar{c} . \bar{c} is usually defined through $\bar{c} = (T - T_u)/(T_b - T_u)$, where T , T_u and T_b are the local temperature, the fresh gases temperature and the burnt bases temperature respectively. As far as two-phase flows are concerned, \bar{c} definition is not so straightforward because of the temperature fluctuations in fresh and burnt gases. In this paper, \bar{c} is used only to determine the statistical characteristics of the flame position to define a reference frame based on the stationary mean flame position. The flame structures were observed through laser tomography with the light source and the camera used for PIV (same magnification ratio). The reacting flow was seeded with olive oil droplets that evaporated near the flame front. The instantaneous 2-D flame surface was obtained by differentiation from the flame images: the dark and bright areas respectively represent burned and unburned states. A total of 1 800 images were used to compute a converged field of the Reynolds averaged progress variable derived from the binary images. The average of the binary images is the probability to find burnt gases (Fig. 2).

To better understand the interaction of the fuel droplets with the flame front, we focused on the measurements of the droplets temperature. The global rainbow technique (GRT), which was introduced by Van Beeck et al. [25], has a large potential of application in actual sprays. It is one of the non-intrusive techniques that can be used to measure average droplets temperature and droplets size distribution under high temperature and high pressure conditions. This technique can be applied to any droplet that is sufficiently transparent. Moreover there is no need to add a

tracer to the liquid phase. If we consider one single droplet (classical rainbow configuration), the main rainbow is generated by the interference between the first internally reflected light and the externally reflected light; it produces a peak of high intensity that is easily identified. The angular location of the rainbow is very sensitive to the droplet refractive index. This means that the location of the rainbow is sensitive to the temperature as well. On top of that the rainbow location is also sensitive to the droplet shape if one single droplet is studied. If we consider several droplets together (GRT configuration), the collective rainbow is created by the summation of a large number of individual rainbows scattered by all the droplets. The analysis of this global rainbow signal gives access simultaneously to both the average droplet temperature and the size distribution. The position of the collective rainbow is especially dependent on the value of the refractive index of the droplets whilst the shape of the global rainbow distribution depends both on the mean diameter and the size distribution. The sensitivity to the particle shape is strongly reduced in that case [29].

Figure 3 displays experimental global rainbow images for *n*-heptane droplets (20 μm in diameter) and the associated intensity profiles (bottom part of the figure). Intensity profiles were processed by a powerful algorithm based on Nussenzweig's theory [30]. This algorithm accurately extracts the value of the refractive index and the associated size distribution. The inversion was carried out in two complementary steps:

- Step 1: the best size distribution was determined for a given refractive index value using a non-negative least squares method.
- Step 2: the refractive index was extracted by minimizing the distance between the measured intensity profile and the computed intensity profile obtained in step 1.

Saengkaew et al. demonstrated the reliability and the accuracy of the global rainbow technique [29]. It was shown that a measurement of the refractive index of the liquid performed with a precision of 10^{-4} leads to a temperature accuracy of 0.2 K. However the temperature obtained from GRT measurements is weighted by the size of the droplets following a $d^{7/3}$ law (i.e. the larger the diameter of the droplets, the most important their contribution to the temperature [31]). It would be better to have the temperature by class of droplet size. However to obtain an average temper-

ature at one point in a flame and to be able to follow the evolution of the temperature with the distance to the flame front was yet a challenge. The results presented for the droplets temperature in this paper must be seen as a first step and the demonstration that temperature measurement is possible in such a configuration by using the global rainbow technique.

The experimental set-up consisted of an emitting and a collecting system that were interdependent. The light source was a continuous laser ($\lambda = 514 \text{ nm}$, $d = 2 \text{ mm}$, $P = 2 \text{ W}$). A first lens collected the light scattered by the particles ($f_1 = 150 \text{ mm}$, $d_1 = 80 \text{ mm}$). The image of the measurement volume was created on a 3 mm in-diameter diaphragm (measurement volume typically equal to 1 mm^3). A second lens ($f_2 = 200 \text{ mm}$, $d_2 = 100 \text{ mm}$) created the image of the focal plane of the first lens on a screen. The signal was recorded by a CCD camera (Kappa, $1050 \times 1400 \text{ pix}$) with a 50 mm lens. The relationship between the scattering angle and its location on the CCD captor was determined by calibration. This relationship was then used to extract from the images the intensity information as a function of the absolute scattering angle. The exposure time was set to the minimum value possible during the experiments (either 110 μs or 220 μs , depending on the signal).

The measurements are recorded at two different heights above the rod: the first height is h_1 at $y = 12 \text{ mm}$ and the second one is h_2 at $y = 26 \text{ mm}$ (Fig. 4, blue dots). The reference point for all the measurements in the non-reactive flow is on the burner centerline. The evolution of the droplet temperature was investigated at level h_1 and level h_2 . First, a relatively small amount of data (100 images at each location) was recorded to obtain the main trends for both flames. Next, four locations were chosen on the first level and scrutinized to obtain the statistical data. 1000 images were recorded at each location. This extensive study of the droplet temperature was performed only in the turbulent flow condition in the presence of the flame. The first measurement was taken on the centerline of the burner exit at each level. Two successive points were separated by a 4° angle (regular mesh, Fig. 5). A sufficient signal-to-noise-ratio was needed to exploit the global rainbow signal. As a consequence, the first effective measurement corresponds to the first exploitable signal, which may be located between two nodes of the regular mesh: it is the first point in space where enough droplets are present in the optical probe to distinguish the rainbow from the noise. Following the same procedure, the last measurement corresponds to the outside limit of the spray (in the fresh gas but on the regular mesh).

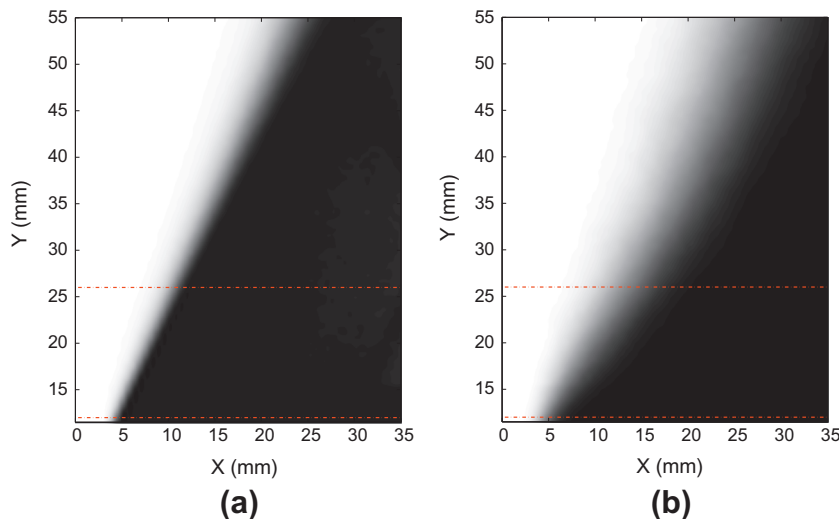


Fig. 2. Image of the mean progress variable with the probed heights (lines). (a) Pseudo-laminar condition (R). (b) Low-turbulence condition (LT).

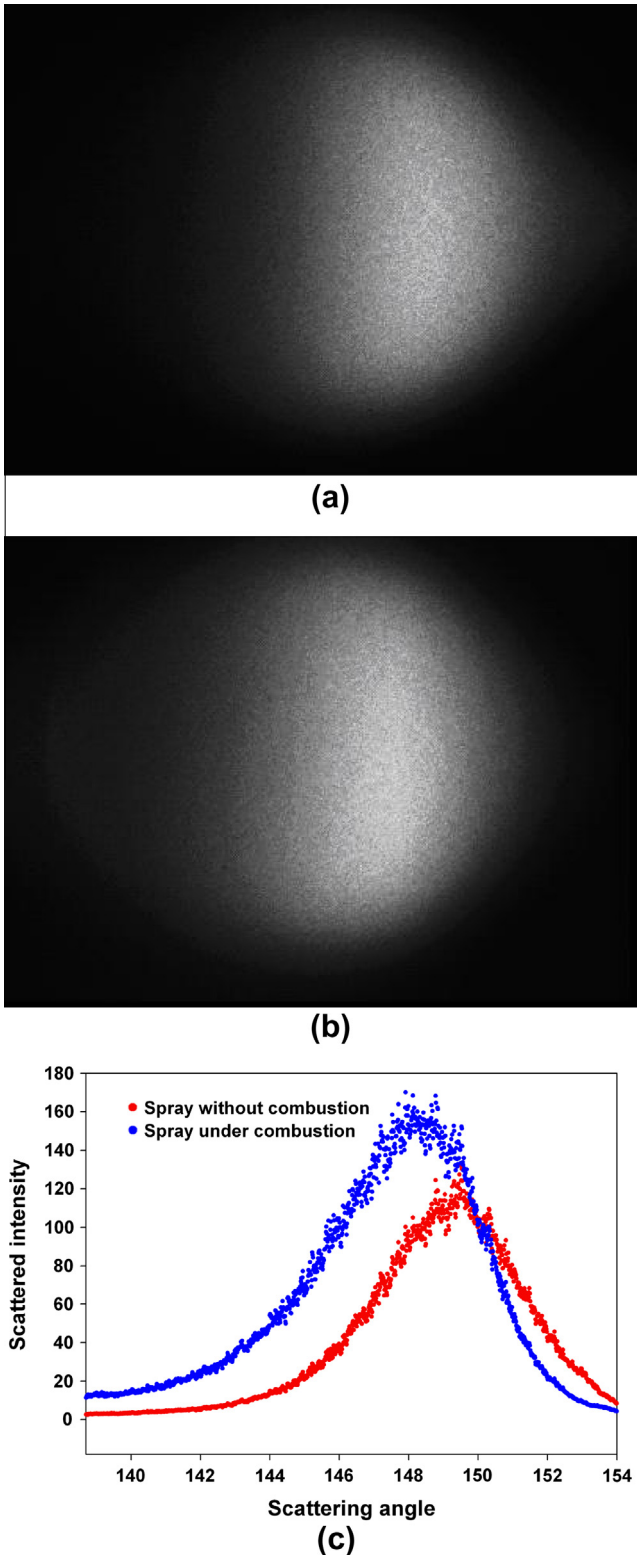


Fig. 3. Experimental global rainbow technique. Images of the rainbow signal (a) without combustion and (b) with combustion. (c) Evolution of the intensity as a function of the scattering angle.

3. Results and discussion

3.1. Characterization of the non-reactive flow

In this paragraph, a brief presentation of the basic properties of non-reactive flows is given. The gas phase properties are detailed

first, then the droplet size distribution. This description is followed by a more in-depth discussion of the liquid temperature distribution inside the spray, which is the core area of our study.

3.1.1. Basic properties of the flow

The turbulent properties of the cold flow were determined through PIV. Results are summarized in Table 1. Only the gaseous phase was considered: the air flow was seeded with olive oil droplets but no fuel was injected. Each record contained 250 images for the pseudo-laminar flow and 500 images for the turbulent flow. The Reynolds number based on the rod diameter and the mean flow velocity in the Y direction (main flow direction) was $Re = 470$. The turbulence intensity was defined according to the average velocity in the main flow direction and the associated fluctuations: $I_T = u'_y / \overline{U}_y$. It reached 5% in the turbulent configuration whereas a residual turbulence of 1% was observed in the pseudo-laminar case.

Droplet size distribution measurements were performed *in situ* and in cold flow conditions (ambient temperature and pressure). The rod was removed from the exit section of the burner. Droplets were injected 600 mm upstream of the rod. The droplets were affected by gravity and were carried by the air flow. The evolution of the Sauter mean diameter was investigated as a function of the spatial position. The height at which measurements were performed had a weak effect on D_{32} (it ranged from 20 μm to 24 μm at the investigated locations). We checked the reproducibility of the measurements. All values of the mean diameter were gathered in a 1 μm -wide interval for six consecutive measurements.

3.1.2. Mean temperature of the fuel droplets

Measurements were recorded at level h_1 ($y = 12$ mm; Fig. 4, blue dot). The reference point for all measurements in the non-reactive flow was located on the burner centerline. We checked the repeatability of the measurements before measuring the droplet temperature distribution in the spray. Ten rainbow images were successively recorded for a given operating condition. The average value of the refraction index was $\bar{m} = 1.3995$. The corresponding distribution of T was monomodal and homogeneous in the non-reactive spray condition (Fig. 6). The resulting distribution was symmetrical (skewness $m_3 = -0.065$) and very narrow around the mean value (standard deviation $\sigma \approx 7 \times 10^{-4}$). All temperature values extracted from the test measurements were grouped in an

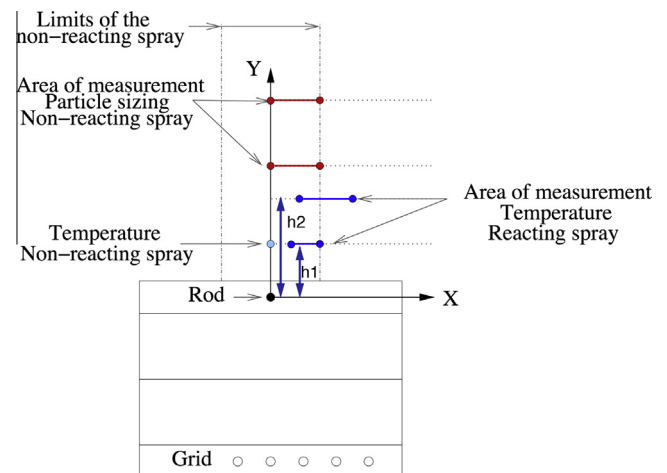


Fig. 4. Sketch of the burner with the location of the measurement points (particle sizing via Malvern, red dots; temperature via GRT, blue dots). (For interpretation of the references to colour in this figure legend, the reader is referred to the web version of this article.)

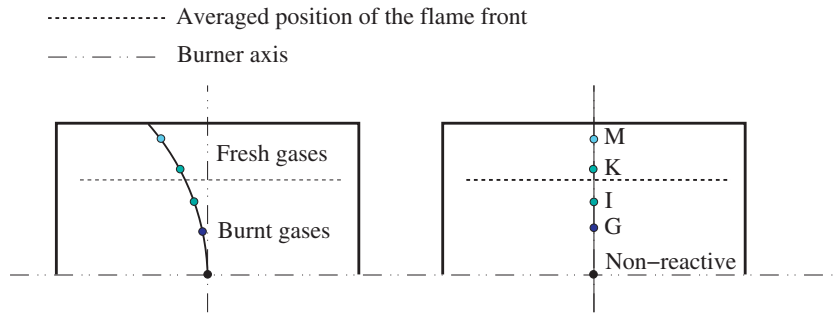


Fig. 5. Sketch of the burner with the location of the GRT temperature measurement points. G: $x = 6.98$ mm; I: $x = 9.31$ mm; K: $x = 11.64$ mm; M: $x = 13.96$ mm.

Table 1
Turbulence properties determined through the PIV experiments.

	Pseudo-laminar R	Turbulent LT
<i>Flow properties</i>		
U_y (m/s)	3.5	3.5
u'_y (m/s)	0.04	0.16
I_T (%)	1.0	4.7
<i>Grid properties</i>		
M (mm)	–	10
Solidity s_b (%)	–	51
L_T (mm)	–	4.47

interval of 3.4 K. This low temperature dispersion is characteristic of spherical droplets.

The absolute temperature value depended on two parameters: the correlation between the refractive index and the temperature, and the measurement of the refractive index itself. The average temperature was equal to 287.4 ± 2 K. This value was quite low compared to the ambient temperature. However, because of the heat transfer between the gas and the liquid, a cooling process first occurred when the liquid was atomized. GRT experiments capture this phenomenon: Saengkaew et al. [29] measured a droplet temperature that was 5 K lower than the ambient temperature in a study of 100 μm diameter mono-disperse methanol droplets.

3.2. Spray temperature distribution

3.2.1. Progress variable fields

As was mentioned in the introduction, two-phase combustion is characterized by various combustion regimes (such as percolation, group, or pre-vaporized combustion), and the corresponding flame

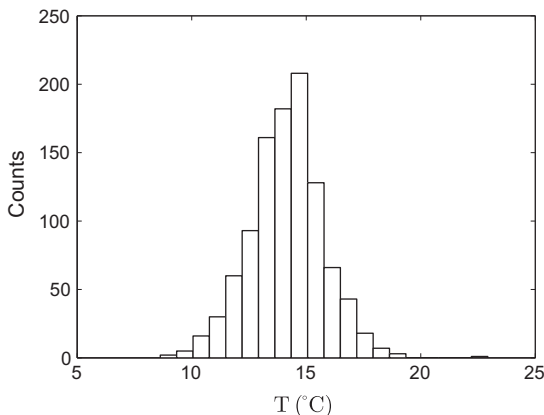


Fig. 6. Fuel droplet temperature distribution around the mean temperature value in the non-reactive spray (1000 images).

structures may be very different [32]. The flames we investigated in this study were situated close to the limit between percolation and pre-vaporized structures (Fig. 7) in the spray combustion diagram [17]. This generally means that most of the fuel droplets were vaporized close to the flame front and only the biggest droplets could pass through it. In this framework approaching premixed combustion, the mean progress variable \bar{c} can be used to study the flame and describe its properties. We present a description of the droplet temperature evolution according to \bar{c} defined previously. For the pseudo-laminar flame, the mean image of the progress variable had linear iso-lines of a mean progress variable \bar{c} (Fig. 8a). This network of curves consisted of straight lines that were slightly diverging from the rod. The iso- \bar{c} were very close to each other, which means that the wrinkling of the flame front remained low. For the turbulent flame, the iso- \bar{c} were no longer linear (Fig. 8b). They followed either a quadratic or a cubic trend. A significant shift between the iso- \bar{c} occurred as the vertical distance to the rod increased: it reflects a strong wrinkling of the flame fronts.

3.2.2. Fuel droplets temperature evolution in the Cartesian coordinates system

Due to the geometry of the configuration and the geometrical properties of the flame, the first location at which it was possible to measure the temperature of the fuel droplets moved away from the burner axis as the distance in the axial direction (vertical) increased. Thus, in the pseudo-laminar configuration, effective data were initially collected at $x = 4.95$ mm on level h_1 and at

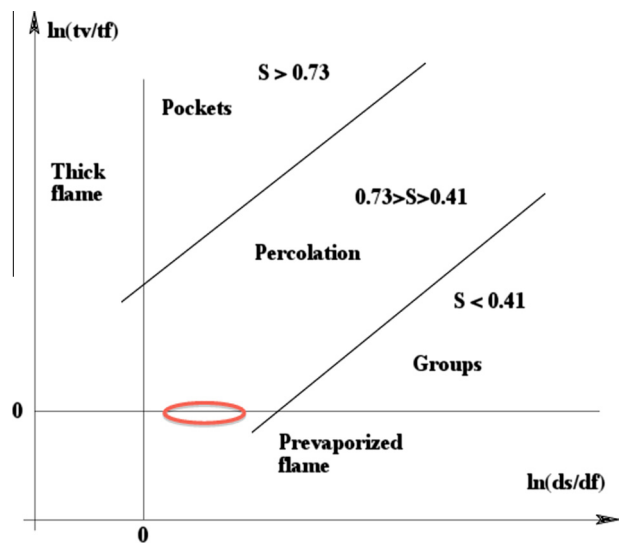


Fig. 7. Spray combustion diagram [17].

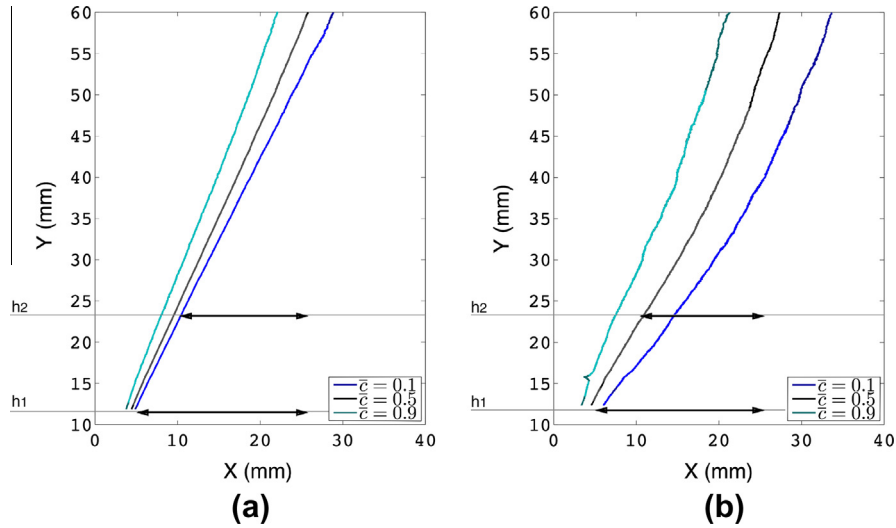


Fig. 8. Localization of the isolines $\bar{c} = 0.1$, $\bar{c} = 0.5$ and $\bar{c} = 0.9$. The black arrows indicate the temperature measurement range. (a) Pseudo-laminar condition. (b) Low-turbulence level condition.

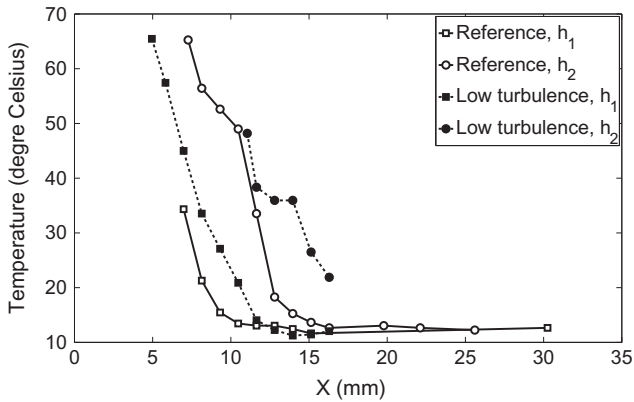


Fig. 9. Evolution of the droplet temperature in the cartesian coordinates system.

$x = 11.05$ mm on level h_2 . The mean value of the refractive index decreased while the distance to the burner axis decreased. We noticed a low dispersion of the measurements, especially for measurements located far away from the flame front (Fig. 9). At this location, the values of the refractive index converged to the value measured in the non-reactive spray. As the location of the measurement moved closer to the flame front, we observed a fast decrease of the refractive index (i.e. increase of the temperature). If we examine the evolution of the droplet temperature at a given axial distance, we notice that the temperature was higher on level h_2 than on level h_1 . To compare the evolution of the temperature on the two levels, the results are presented as a function of the mean progress variable (evolution of the droplet temperature inside the turbulent flame brush).

3.2.3. Fuel droplets temperature evolution in the flame coordinates system

Measurements were recorded from $\bar{c} = 0$ to $\bar{c} \approx 0.8$. The number of exploitable images decreased drastically at each location where $\bar{c} > 0.5$. The temperature of the droplets was higher on the first level h_1 (Fig. 10). This observation may be surprising, in particular if we consider that the droplets begin heating up at the time of their injection into the flow and continue to rise in temperature until their total vaporization. A droplet on level h_2 should

therefore have a higher temperature than a droplet on level h_1 . We propose several explanations for this phenomenon. To begin with, level h_1 was closer to the rod than level h_2 . This rod was not artificially heated. However it may have experienced a slight temperature increase due to the surrounding heat radiation. Therefore some heat could have been released and could have contributed to the heating of the fuel droplets. Furthermore, particle tracking through direct numerical simulation of the configuration (not presented in this paper) showed that the droplets that reach level h_2 were originally located at the external limit of the spray (in fresh gases). Thus these particles were located further away from the flame front during their transport by the gaseous flow. It is also likely that the gas temperature was lower at some distance from the flame front.

3.2.4. Statistical data

We recorded 1000 images of the flame in the low-turbulence condition. Four locations were chosen locations on level h_1 (from fresh to burnt gases: M_{h_1} , K_{h_1} , I_{h_1} , and G_{h_1} ; see Fig. 11 and Table 2). Histograms present the evolution of the temperature index versus the location of the optical probe in the flames. The reference measurement in the non-reactive spray is shown in black. The distribution of the temperature is narrow and Gaussian.

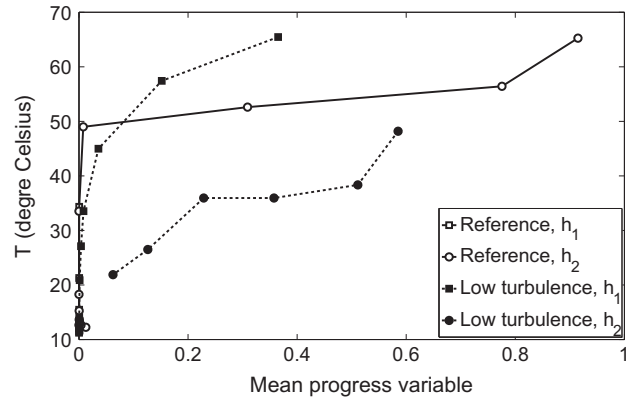


Fig. 10. Evolution of the droplet temperature in the local coordinates system as a function of the mean progress variable. Case h_1 is always positioned at $\bar{c} = 0$ because measurement is done in the fresh gases (Fig. 8).

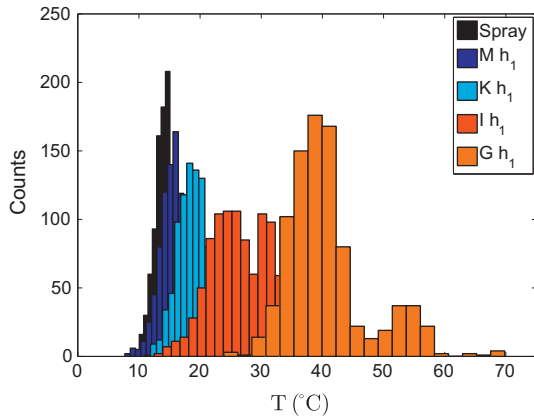


Fig. 11. Distribution of the temperature (1000 samples at each location on level h_1).

Table 2

Detailed temperature measurements. Position of the four locations chosen for detailed measurements in the Cartesian grid. Mean value of the progress variable, droplet temperature rise, and associated standard deviation.

Location	G_{h_1}	I_{h_1}	K_{h_1}	M_{h_1}
x (mm)	6.98	9.31	11.64	13.96
\bar{c}	0.49	0.20	0.08	0.02
$\overline{\Delta T}$ (K) \pm 0.2	23.3	39.0	9.9	17.1
σ (K)	3.6	4.4	3.6	2.2

Measurements taken at location M_{h_1} (13.96 mm from the flame axis) are presented in cyan. The value of the mean progress variable associated with this location was $\bar{c} = 0.02$. The mean temperature of the droplets was $\bar{T} = 288.8$ K, which corresponds to an increase of 1.4 K compared to the temperature of the non-reactive spray. The dispersion around the mean value was 2.2 K.

Measurements recorded at location K_{h_1} (11.64 mm from the flame axis) are shown in turquoise blue. The value of the mean progress variable associated with this location was $\bar{c} = 0.08$. The mean temperature of the droplets was $\bar{T} = 292.5$ K, which corresponds to an increase of 5.1 K (dispersion of 3.0 K). According to the values of \bar{c} , more than 90 % of the measurements at M_{h_1} and K_{h_1} correspond to the measurements obtained in fresh gases. The extracted distributions are Gaussian and mono-modal. However, the distributions became larger as the radial distance to the flame front was reduced.

Measurements taken at location I_{h_1} (9.31 mm from the flame axis) are presented in red. The value of the mean progress variable associated with this location was $\bar{c} = 0.20$. From a statistical point of view, 1/5 of the measurements were located in burnt gases. Unfortunately, due to the exposure time during the experiments, it is impossible to determine from these records whether the location of the measurement was located in fresh gases or in burnt gases. The width of the distribution continued to increase (27 K), and the distribution became bimodal (Fig. 12, Table 3). We can assume that the shape of this distribution is the addition of two Gaussian curves. This phenomenon can be explained as follows: The first peak is due to the location of the fuel droplets in the fresh gases, which was quite far from the flame front (moderate temperature). The second is the result of fuel droplets very close to the flame front, which was sometimes located in the burnt gases (higher temperature). At this location the mean temperature was 9.9 K higher than the temperature of the majority of the values in the distribution (69.6 % of the global population) and 17.1 K higher than the minority of the distribution values. The mean tempera-

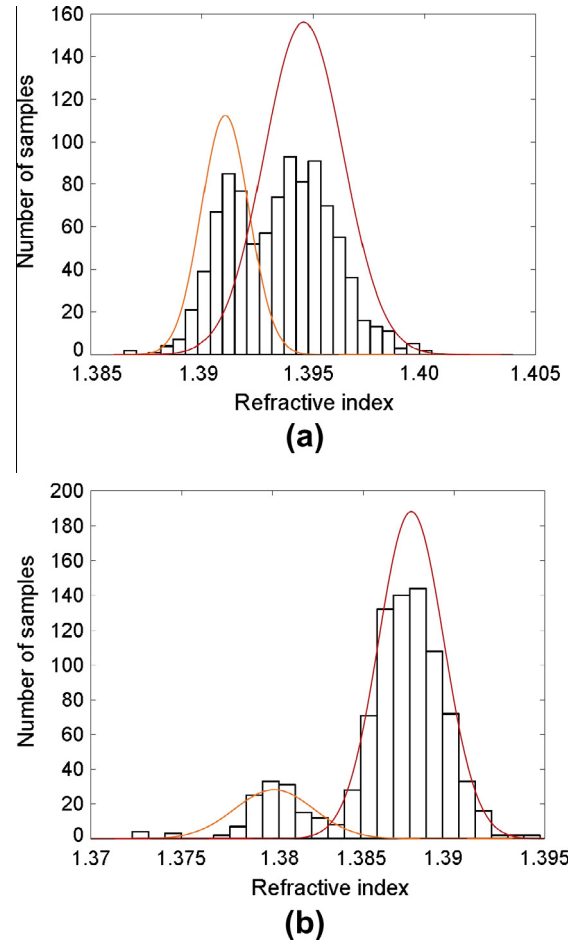


Fig. 12. Processing of the bimodal refractive index distribution histograms as the superposition of two gaussian distributions. (a) I_{h_1} , (b) G_{h_1} .

ture associated with the two peaks was $\bar{T} = 297.3$ K (dispersion around the mean value of 3.6 K) and $\bar{T} = 304.5$ K (dispersion of 2.2 K).

The bimodal shape of the distribution was confirmed by the measurements at location G_{h_1} (6.98 mm from the flame axis) presented in orange. The mean progress variable at this location was $\bar{c} = 0.49$, which means that it was equiprobable to measure the refractive index in fresh and burnt gases. The mean variation of temperature for the two peaks was 23.3 K (84.6% of the global population) and 39 K. This corresponds to a mean temperature of $\bar{T} = 310.7$ K (dispersion of 3.6 K) and $\bar{T} = 326.4$ K (dispersion of 4.4 K).

The highest temperature extracted from the experimental results was close to 343 K. This value remained lower than the boiling temperature of *N*-heptane ($T_b = 371.6$ K). Unfortunately, it was impossible to reach higher values of \bar{c} because measurements would need to be performed essentially in the burnt gases, where very few droplets are present. In that case, the exposure time should be drastically increased; the signal-to-noise ratio would then be reduced, and the quality of records would be altered.

Table 3

Effect of a bimodal shape on droplet temperature: post-processing of the droplet temperature mean value.

	G_{h_1}	I_{h_1}		
$\overline{\Delta T}$ (monomodal processing) (K)	12.1	26.1		
$\overline{\Delta T}$ (bimodal processing) (K)	39.0	23.9	17.1	9.9
Proportion of each distribution (%)	30.4	69.6	15.38	84.62

4. Conclusion

In two-phase combustion, specific information on both liquid and gas phase temperatures is needed to characterize heat transfer on one hand and, on the other hand, to develop and validate appropriate vaporization, ignition and combustion models that consider the thermodynamical processes at the liquid interface. In this context, we conducted an experimental study of two-phase flames (*N*-heptane/air) at atmospheric pressure. Quantitative measurements were recorded to analyze the interaction of fuel droplets and flame fronts in terms of fuel droplet temperature distributions. The evolution of the fuel droplet temperature in the vicinity of the flame front was determined through the global rainbow technique. This technique is able to provide a quantitative measurement of the mean fuel droplet temperature in a measurement volume of 1 mm³. Temperature statistics were then computed from a set of 1000 rainbow images. For the first time, this technique was successfully tested in a V-shape flame configuration. Furthermore, the flame front structure was obtained from tomographic records for two flow conditions (laminar and low-turbulence) and characterized by the mean progress variable \bar{c} . Statistics in the non-reactive flow condition of the velocity fields, the fuel droplet size distribution, as well as the fuel droplet temperatures are also provided. The evolution of the fuel droplets temperature are reported in the physical space across the flame brush at two heights above the rod. The droplet temperature rises slowly far from the flame fronts. This is followed by a sudden rise in temperature as the droplets arrive in the vicinity of the flame brush. The same results were observed in the mean progress variable space, where the mean fuel droplet temperature increased with \bar{c} . Due to the small number of droplets available at $\bar{c} > 0.8$, it was impossible to determine the droplet temperature for higher values of the mean progress variable. Fuel temperature distributions were also obtained from the 1000 rainbow images. Initially the fuel droplet temperature distribution was mono-modal for low mean progress variable values. It became bimodal when the measurement volume shifted towards the burnt gases ($\bar{c} > 0.2$). Our analysis demonstrates that it is important to consider this bimodal aspect in the computation of the mean temperature. The bimodal shape of the histograms is explained by the contributions of droplets located in fresh gases as well as droplets located either at the flame front or in burnt

gases. The contribution of the droplets located in fresh gases became less important as the value of \bar{c} increased.

Acknowledgment

Part of this work was supported by ACI-Jeune Chercheur-CNRS.

References

- [1] G. Chen, A. Gomez, *Comb. Flame* 110 (1997) 392–404.
- [2] G. Chen, A. Gomez, *Proc. Comb. Inst.* 24 (1992) 1531–1539.
- [3] H. Nomura, M. Hayasaki, Y. Ujiie, *Proc. Comb. Inst.* 31 (2007) 2265–2272.
- [4] M. Mikami, K. Yamamoto, O. Moriue, N. Kojima, *Proc. Comb. Inst.* 30 (2005) 2021–2028.
- [5] C. Presser, A. Gupta, H. Semerjian, *Comb. Flame* 92 (1993) 25–44.
- [6] T. Marchione, S. Ahmed, E. Mastorakos, *Comb. Flame* 156 (2009) 166–180.
- [7] P. Arias, H. Im, P. Narayanan, A. Troune, *Proc. Comb. Inst.* 33 (2011) 2591–2597.
- [8] Y. Wang, C. Rutland, *Comb. Flame* 30 (2005) 893–900.
- [9] R. Stauch, S. Lipp, U. Maas, *Comb. Flame* 145 (2006) 533–542.
- [10] C. Wang, K. Shy, L. Lieu, *Comb. Sci. Tech.* 118 (1996) 63–78.
- [11] Q. Khan, S. Baek, H. Ghassemi, *Comb. Sci. Tech.* 179 (2007) 2437–2451.
- [12] S. Aggarwal, *Prog. Energy Comb. Sci.* 24 (1998) 565–600.
- [13] Z. Bouali, C. Pera, J. Reveillon, *Comb. Flame* 159 (2012) 2056–2068.
- [14] J. Reveillon, L. Vervisch, *J. Fluid Mech.* 537 (2005) 317–347.
- [15] H.H. Chiu, H.Y. Kim, E.J. Croke, *Proc. Comb. Inst.* 19 (1982) 971–980.
- [16] S.H. Chang (Ed.), *Transport Phenomena in Combustion*, Taylor and Francis, 1996.
- [17] R. Borghi, in: [16] S.H. Chang (Ed.), *Transport Phenomena in Combustion*, Taylor and Francis, 1996, pp. 1–18.
- [18] C. Amiel, Ph.D. thesis, Ecole Nationale Supérieure de l'Aéronautique et de l'Espace, Toulouse, France, 2003.
- [19] R. Chang, J. Campillo, *Optical Processes in Microcavities*, *Advanced Series in Applied Physics*, vol. 3, World Scientific Publishing, 1996.
- [20] G. Chen, M. Mazunder, R. Chang, J. Swindal, W. Acker, *Prog. Energy Combust. Sci.* 22 (1996) 163–188.
- [21] T. Müller, G. Grünefeld, V. Beushausen, *Appl. Phys. B* 70 (2000).
- [22] G. Castanet, A. Delconte, F. Lemoine, L. Méès, G. Gréhan, *Exp. Fluids* 39 (2005) 431–440.
- [23] N. Roth, K. Anders, A. Frohn, *Appl. Opt.* 30 (1991).
- [24] S. Saengkaew, T. Charinpanikul, C. Laurent, Y. Biscos, G. Lavergne, G. Gouesbet, G. Gréhan, *Exp. Fluids* 48 (2010) 111–119.
- [25] J. Van Beeck, D. Giannoulis, L. Zimmer, M. Riethmuller, *Opt. Lett.* 24 (1999) 1696–1698.
- [26] O. Degardin, B. Renou, A. Boukhalfa, *Exp. Fluids* 40 (2006) 452–463.
- [27] N. Mazellier, L. Danaila, B. Renou, *J. Turb.* 11 (2010) 1–30.
- [28] F. Scarano, M. Riethmuller, *Exp. Fluids* 26 (1999) 513–523.
- [29] S. Saengkaew, G. Godard, J. Blaisot, G. Gréhan, *Exp. Fluids* 47 (2009) 839–848.
- [30] S. Saengkaew, Ph.D. thesis, Faculty of Engineering, Chulalongkorn University and University of Rouen, 2005.
- [31] S. Saengkaew, V. Bodoc, G. Lavergne, G. Gréhan, *Opt. Commun.* 286 (2013) 295–303.
- [32] J. Reveillon, L. Vervisch, *J. Fluids Mech.* 537 (2005) 317–347.